Methodology for the Synthesis of Methacrylate Monomers Using Designed Single Mode Microwave Applicators

Adam A. Dundas[a,b], Andrew L. Hook[b], Morgan R. Alexander[b], Sam W. Kingman[a], Georgios Dimitrakis*[a] and Derek J. Irvine*[a]

[a]. Department of Chemical and Environmental Engineering, Faculty of Engineering, University of Nottingham, NG7 2RD

[b]. Advanced Materials and Healthcare Technologies, School of Pharmacy, University of Nottingham, NG7 2RD

*. Corresponding authors

Supplementary Information

Experimental Methods

Conventional Heating

The typical protocol for conventional heating was as follows. Butyl methacrylate (7.5 g (53 mmol), was added to 38 mmol of the desired alcohol into a 50 ml round bottom vessel with an extended neck (for comparison to the conventional microwave method). 0.5 mmol of titanium butoxide was then added to the reaction mixture. The reaction vessel was placed in a heating mantle on a hot plate and heated to 160 ˚C with 500 rpm stirring. The reaction was heated for 150 minutes were upon the reaction was left to cool and sampled for NMR.

Conventional Microwave Heating

The typical protocol for conventional microwave heating was as follows. Butyl methacrylate (7.5 g 53 mmol), was added to 38 mmol of the desired alcohol into a 50 ml round bottom vessel with an extended glassware neck. 0.5 mmol of titanium butoxide was then added to the reaction mixture. The extended neck was required for this method as the choke for microwave (which prevents microwave leakage) means conventional glassware cannot be used. The reaction was then heated to 160 ˚C for 150 minutes using a Sairem Miniflow 200SS at 150 W were upon the reaction was left to cool and sampled for NMR.

Microwell Heating

The typical protocol for microwell heating was as follows. Butyl methacrylate (7.5 g 53 mmol), was added to 38 mmol of the desired alcohol and 0.5 mmol of titanium butoxide. This reaction mixture was then added into the reaction vessel shown in Figure S6. This was then attached to an impedance matching trombone to help match the input signal to the reactants. The input power (typically used 80 W) was used to heat the reaction to 160 ˚C again using the Sairem Miniflow 200SS as a power source. After heating the reaction was left to cool and sampled for NMR.

NMR Analysis

Characterisation *via* Nuclear Magnetic Resonance Spectroscopy: ^{1}H NMR spectroscopic analyses were recored at 25 °C using Bruker AV-400 MHz spectrometers. Samples were dissolved in deuterated chloroform ($CDCl_3$; 10 mg ml^{-1}) to

which chemical shifts are referenced (residual chloform at 7.26 ppm). Analysis of the spectra was carried out using MestReNova.

Supplementary Figures

The archetypal HTP test-bed geometry can be regarded as the multi-well plate system shown in Figure S1. These plates have well capacities that are somewhere between 1 and 5 mLs. Figure 1 concisely shows what is HTP target is for scaling out the individual reactor designed and tested in this paper. It the positioning of several single wells adjacent to each other to form a multiple reactor bed. The experimental work presented in this manuscript details that a 10-20 mL single-well, microwave reactor has the potential to, in essence, become the equivalent of one of the well in the plate above by mitigating the issues, highlighted above, that plague conventionally heated well plates when they are increased in scale.

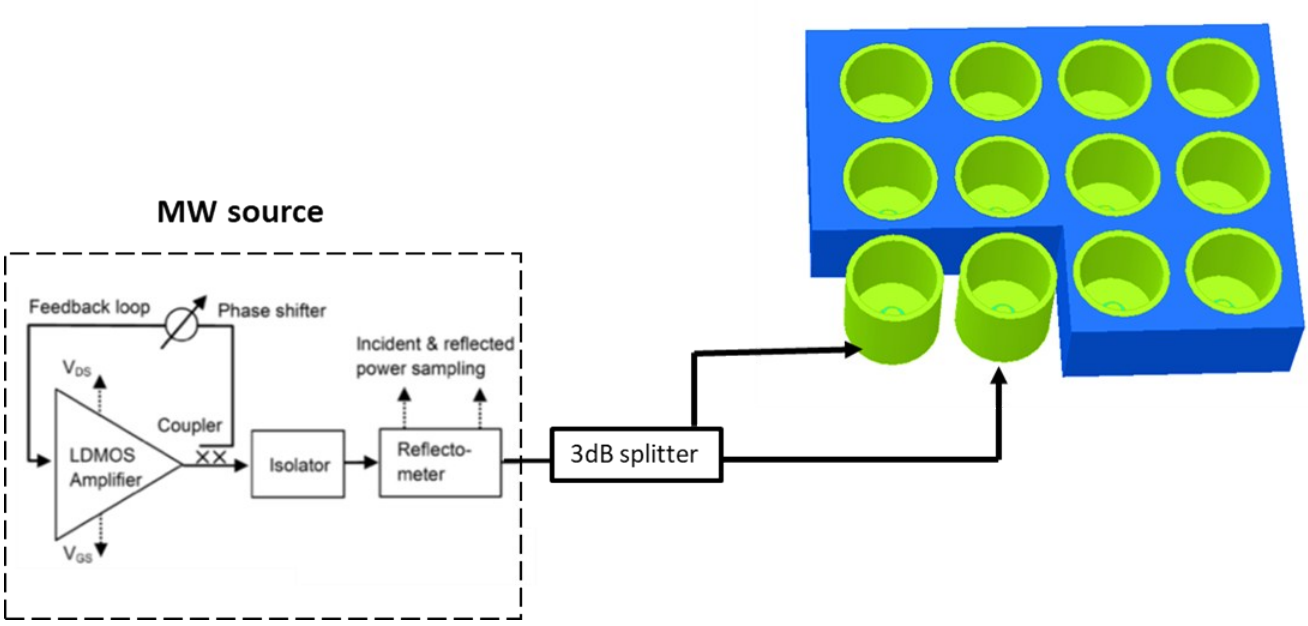

Figure S1: Figure showing the proposed multi-well system where a single microwell forms part of a larger microwave array system.

Open top vials can be used in a standard single mode cavity. However, these must have a long-necked piece of glassware to extend the vial beyond the top of the cavities choke system. In practice, calculation determined that this neck had to be much longer in the conventional system than the micro-well vessels head-space volume discussed above.

The well geometry of the micro-well reactor was optimised by choosing a suitable radius that allowed a high-power density distribution whilst maintaining a large enough reaction mixture to do a range of subsequent analysis with novel monomers produced by the transesterification process. Shown in Figure S2 is the power density distribution associated to wells with differing radii of 8.13 mm,15 mm and 20 mm respectively.

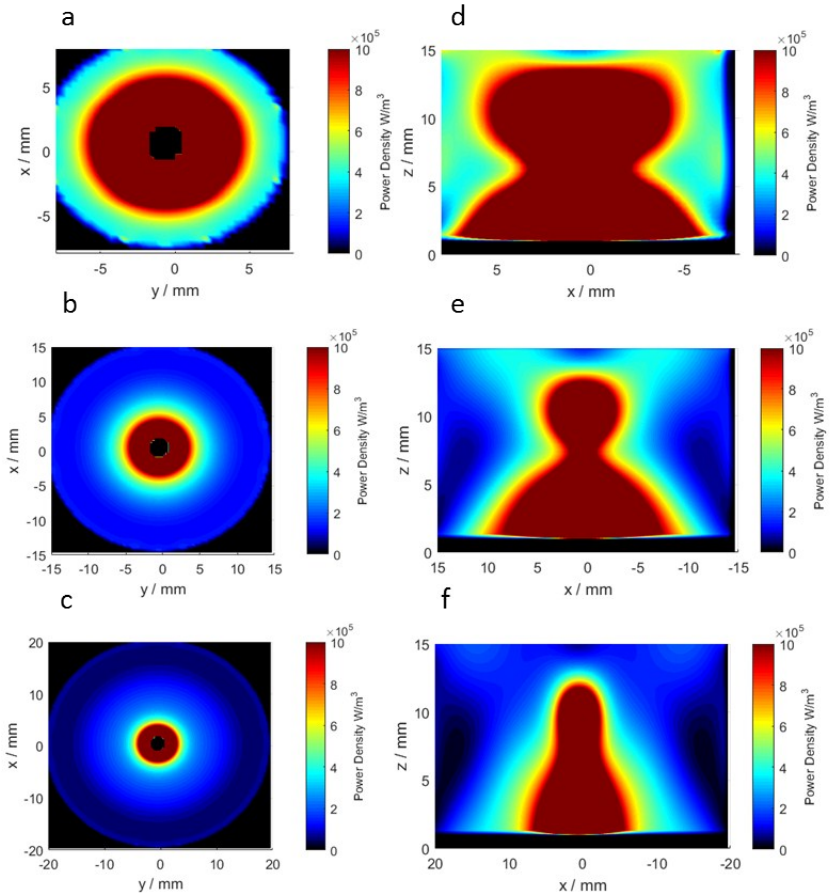

Figure S2: Figure showing the effect of changing the reactor size on power density distribution with a,b and c showing the XY = 10 mm power density for reactor sizes of 8.13, 15 and 20 mm respectively. Figures d,e and f show the XZ = 2.8 mm power density distribution for reactor sizes of 8.13, 15 and 20 mm respectively. All geometries were performed with a cylindrical antenna with length equal to 10 mm.

It was observed that despite the 24-well sized reactor offering a higher power density distribution, that a larger reactor could be used at a slight compromise of power density distribution for more material to be processing during each batch reaction. However when going to a radius of 20 mm, the power density is shown to start to not propagate radially, therefore a reactor with radius 15 mm was chosen as an optimum well radius design, which was able to propagate 2.45 GHz microwaves to a sufficient amount of the load material.

In addition to well geometry, the antenna was designed such that a high-power density distribution was achieved as uniformly as possible. First, the antenna length was optimised at 10 mm, with both longer (15 mm) and shorter (5 mm) antennas unable to achieve a uniform field as demonstrated by an antenna with length 10 mm (Figure S2).

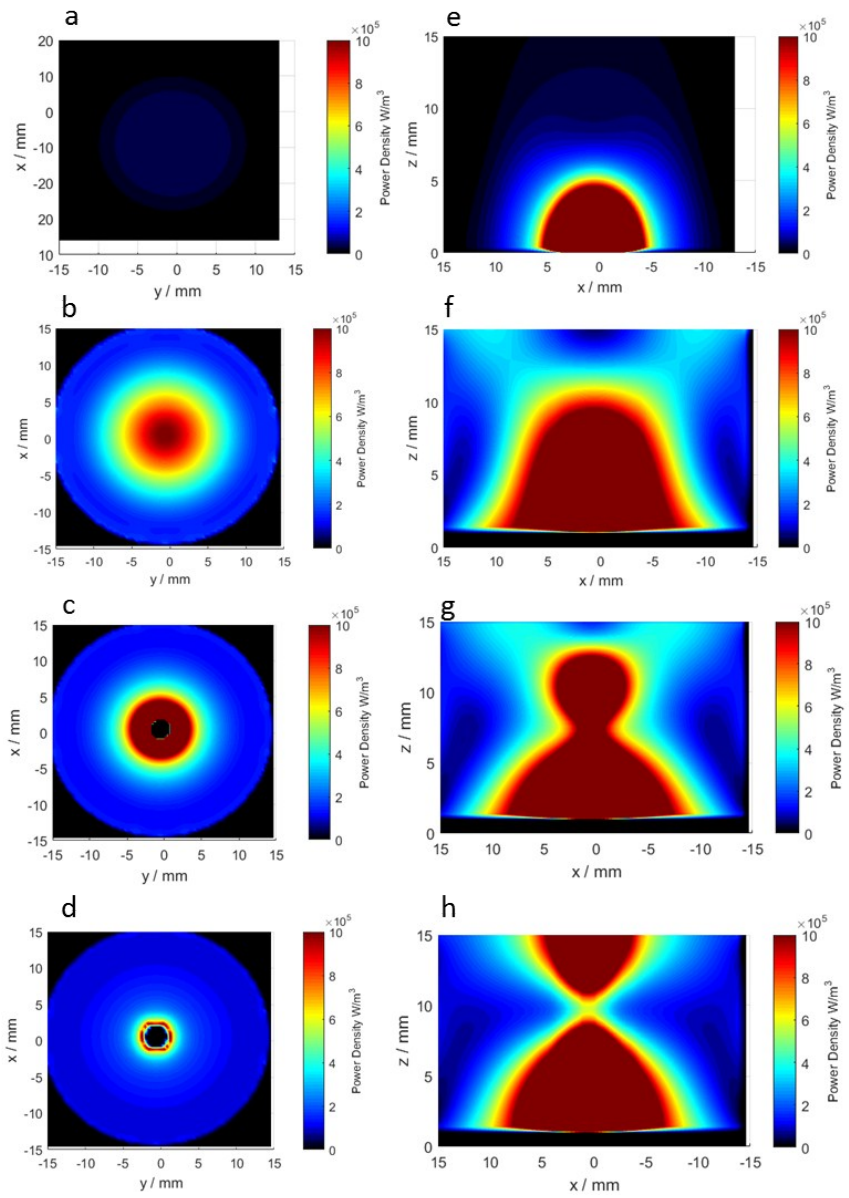

Figure S3: Power density distributions for different length antenna designs showing an XY slice at 10 mm on the left (figures a, b, c and d) and an XZ slice at 2.6 mm on the right (figures e, f, g and h). Designs shown in figure a and e represent simulations performed with no antenna. Designs shown in figure b and f represent simulations performed with a cylindrical antenna of length 5 mm. Designs shown in figures c and g represent simulations performed with a cylindrical antenna of length 10 mm. Designs shown in figures d and h represent simulations performed with a cylindrical antenna of length 15 mm. Simulations were performed with a mesh containing 650,000 cells and performed for 30,000 iterations.

As shown above, using a longer antenna allows for coupling of microwaves to deeper parts of reaction mixture compared to shorter antennas, especially the 5 mm antenna, however the longer antenna does not offer as uniform power density distribution as the 10 mm long antenna shown in Figure S3(c and g).

After optimising the length of the antenna, the shape was modified to observe effects of antenna geometry on the power density distribution. This included a standard cylindrical antenna, a cylindrical antenna with point end, an inverted cone antenna and a cylindrical antenna that has both ends tapered (Figure S4).

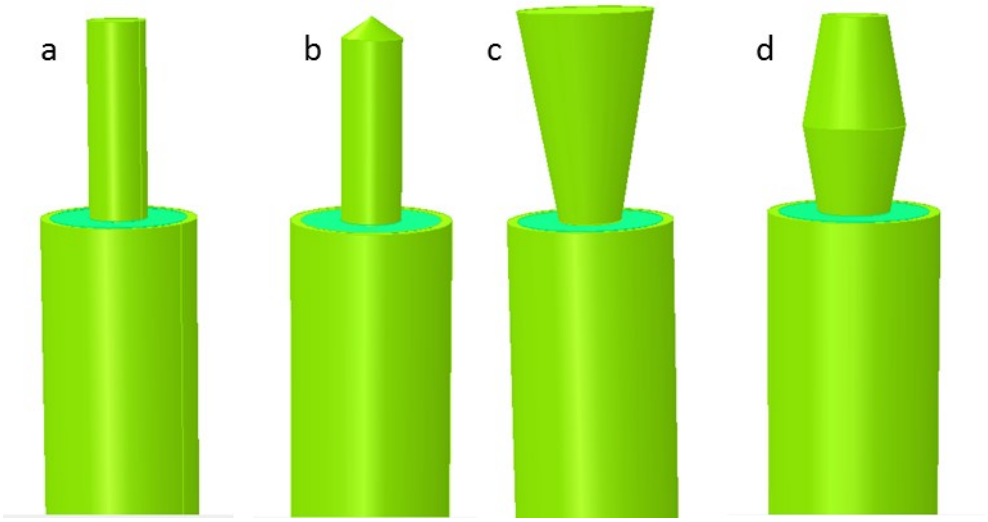

Figure S4: Antenna shape designs showing (a) standard cylindrical antenna (b) pointed antenna (c) inverted cone antenna (d) tapered cylindrical antenna. All antennas were at the same length of 10 mm

Antenna designs were simulated in a 15-mm radius well all at the same antenna length of 10 mm, and design comparisons can be shown in Figure S4.

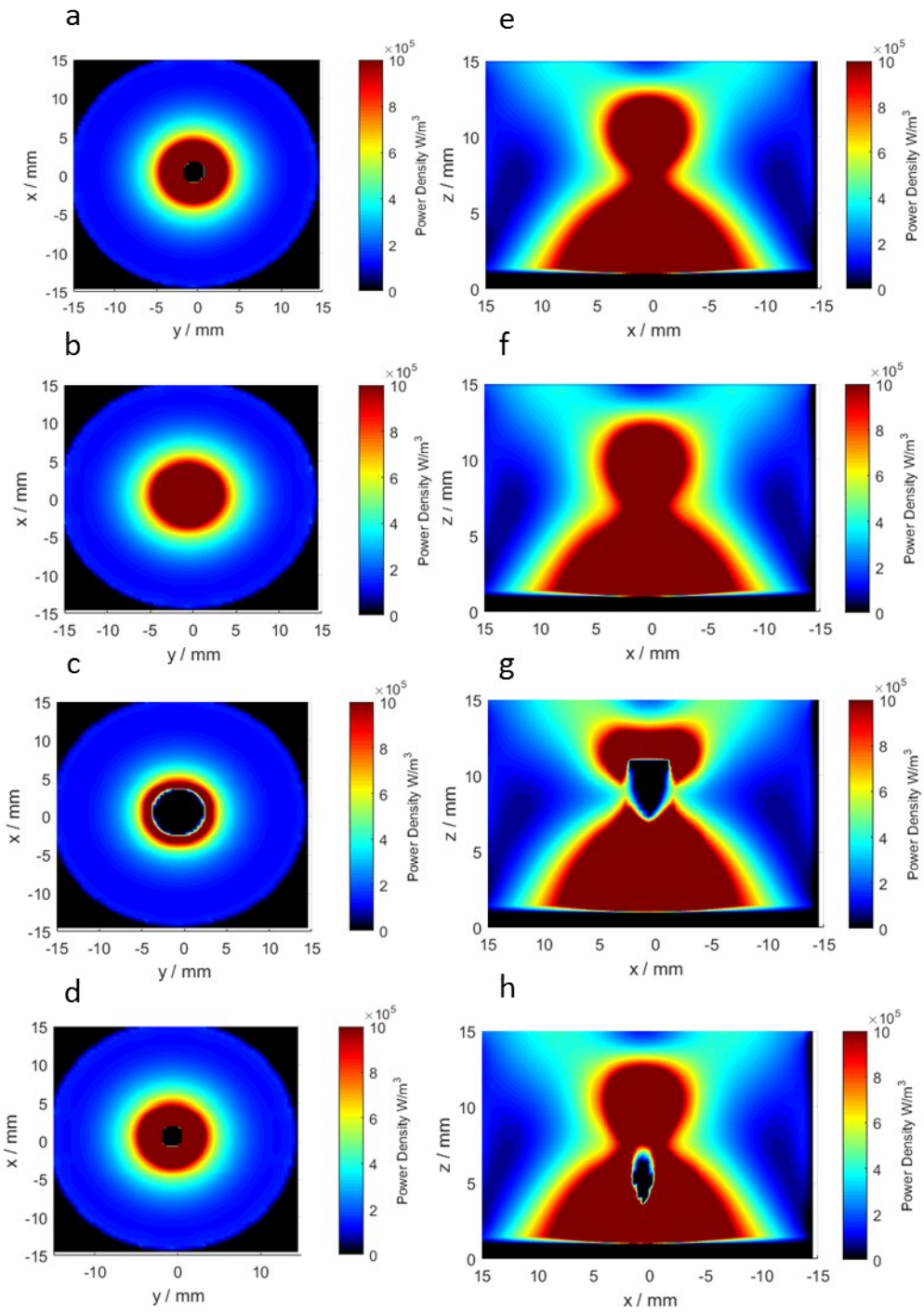

Figure S5: Power density distributions for antenna designs showing an XY slice at 10 mm on the left (figures a, b, c and d) and an XZ slice at 2.6 mm on the right (figures e, f, g and h). Designs shown in figure a and e represent simulations performed with a cylindrical antenna. Designs shown in figure b and f represent simulations performed with a pointed antenna. Designs shown in figures c and g represent simulations performed with an inverted cone antenna. Designs shown in figures d and h represent simulations performed with a tapered cylindrical antenna design. Simulations were performed with a mesh containing 650,000 cells and performed for 30,000 iterations.

As shown above, there was limited effect of changing the antenna geometry with the geometries shown in Figure S4, and therefore the simple cylindrical design was taken forward for the manufacture of the micro-well reactor to increase

the ease of manufacture. The manufactured micro-well reactor can be shown in Figure S6. Figure S6 contains a picture of the whole microwave reactor including the "stem" of the reactor in which the coaxial line is located. The "stem" is rectangular rather than cylindrical to facilitate ease of manufacture and in fact has no influence in the performance of the system as long as internally it contains a coaxial line with 50 Ω impedance. For the purposes of the electromagnetic simulation only the internal, electrically active parts of the reactor need to be simulated and these are the sections has been included in Figure 3.

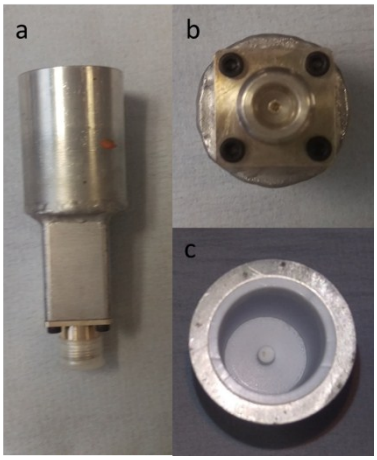

Figure S6: Manufactured Micro-well reactor showing (a) whole reactor including 40 mm coaxial section and 50 mm cylindrical reaction vessel (b) N-type connector used for connecting to high-power coaxial cable (c) top-view showing protruding antenna and PTFE sheath covering inside of the reactor

Well-designed microwave reactors tend to dissipate heat directly into the material, achieving what is referred to as volumetric heating. In practice, volumetric heating often results in inverse temperature profiles, i.e. the interior of the sample is hotter than the exterior.[1] This has been attributed to the fact that the reactor walls are in contact with the cooler surroundings. By comparison, conventional reactors rely on thermal conduction and convection mechanisms to transfer heat from the wall to the reactants, i.e. the samples exterior is heated first before the temperature can penetrate in the rest of the material. As a result, the conventional heating processes are typically a lot slower that with microwave heating. It is these fundamentally different heating mechanisms that are the basis for the different power requirements between the microwave and conventional reactors and result in the conventional ones typically requiring much higher powers.

In the micro-well the reactants are not in direct contact with the metal structure but instead there is a PTFE insert (seen in Figure S6) which lines the interior of the well. This has been added for three reasons (a) to impart a level of chemical resistance to the reactor, (b) to prevent any liquid ingress down into the coaxial cable "stem" and (c) to provide a basic level of thermal insulation (See Figure 3b).

In our new design, the reactor is in-fact the cavity. Thus, it is possible to use such an open format, as long as the reactor length is sufficient that the open top section (i.e. the head-space between the top of the liquid and the top edge of the reactor) performs as a choke. In this way the electromagnetic energy does not leak from reactor body. Thus, as a result, the reactor is smaller and more efficient as it doesn't suffer so heavily from internal condensation of the by-product alcohol. It also can handle varying internal volumes of reaction mixture without redesign provided that the recommended head-space area is maintained or exceeded. To ensure that safety protocols were met, simulations were performed to examine the power density of microwaves at the opened end of the Microwell. The cut-off frequency of the fundamental excited mode (TE_{11}) was calculated and a well diameter chosen such that microwaves should not leak. An exterior port was placed above the microwell and the S21 parameter was observed to see microwaves coupling from the power source to the exterior port. Figure S7 shows that over a frequency range of 2 – 5 GHz, the emitted microwaves are well below the 5 mW/cm^2 maximum permissible dosage limit.

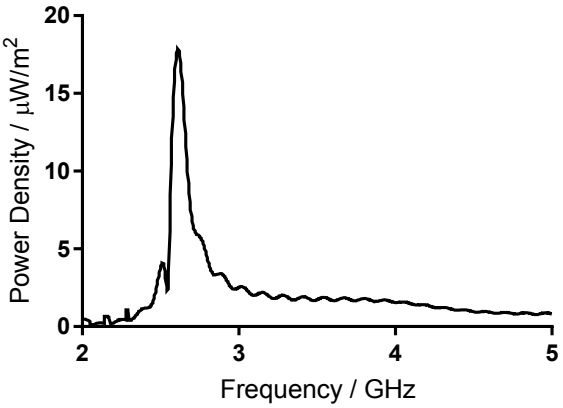

Figure S7: Frequency sweep between 2 and 5 GHz showing power density leaked to exterior of Microwell design

To test the how effective the Micro-well was at synthesising novel methacrylate monomers, a series of monomers were synthesised in conventional, microwave and micro-well methodologies and analysed using a Bruker 400 MHz NMR spectrometer. This involved observing the change in chemical environment of protons from the alcohol to the novel methacrylate. Shown below are the NMR for CyDMA for conventional, microwave and micro-well respectively.

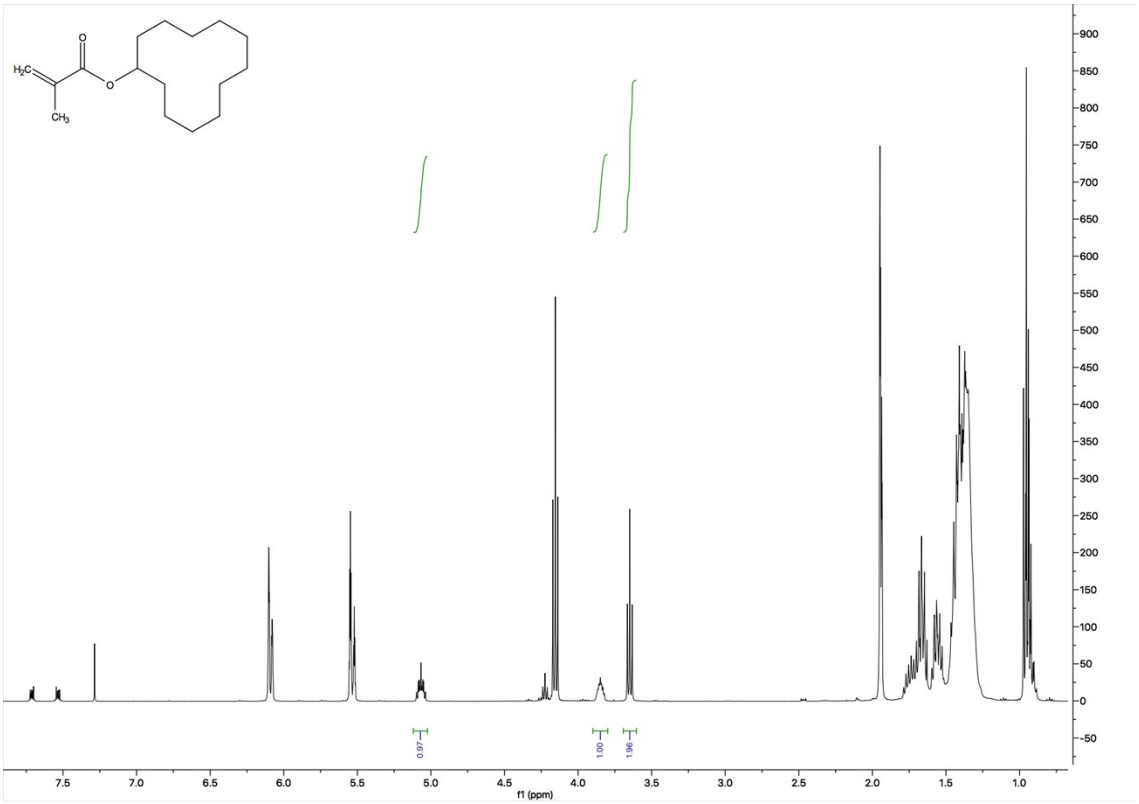

Figure S8: 1H NMR of conventional CyDMA after 150 mins of heating at 160 ˚C. Conversion shown to be 48 % by comparing proton peak change in chemical environment

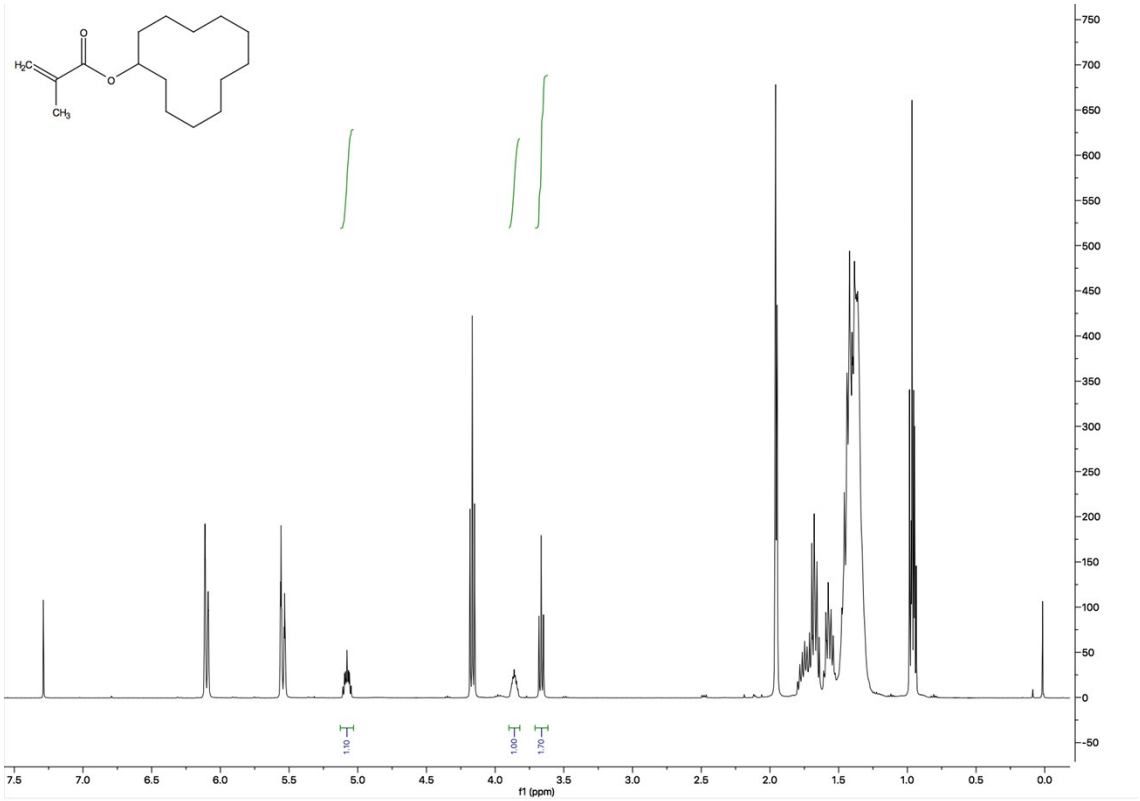

Figure S9: 1H NMR of microwave-heated CyDMA after 150 mins of heating at 160 ˚C. Conversion was shown to be 52 % by comparing proton peak change in chemical environment

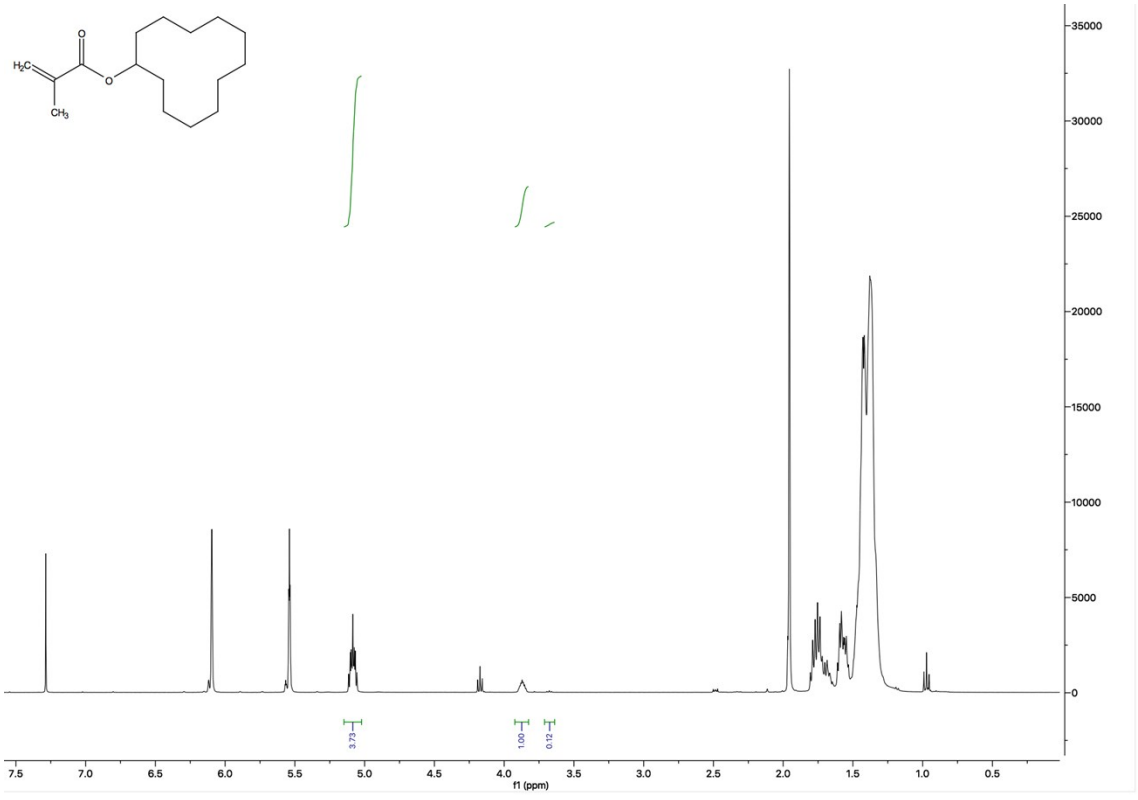

Figure S10: 1H NMR of micro-well CyDMA after 150 mins of heating at 160 ˚C. Conversion was shown to be 78 % by comparing proton peak change in chemical environment

Following the experimentation of CyDMA, the same process was repeated for CiMA, MpMA and LMMA.

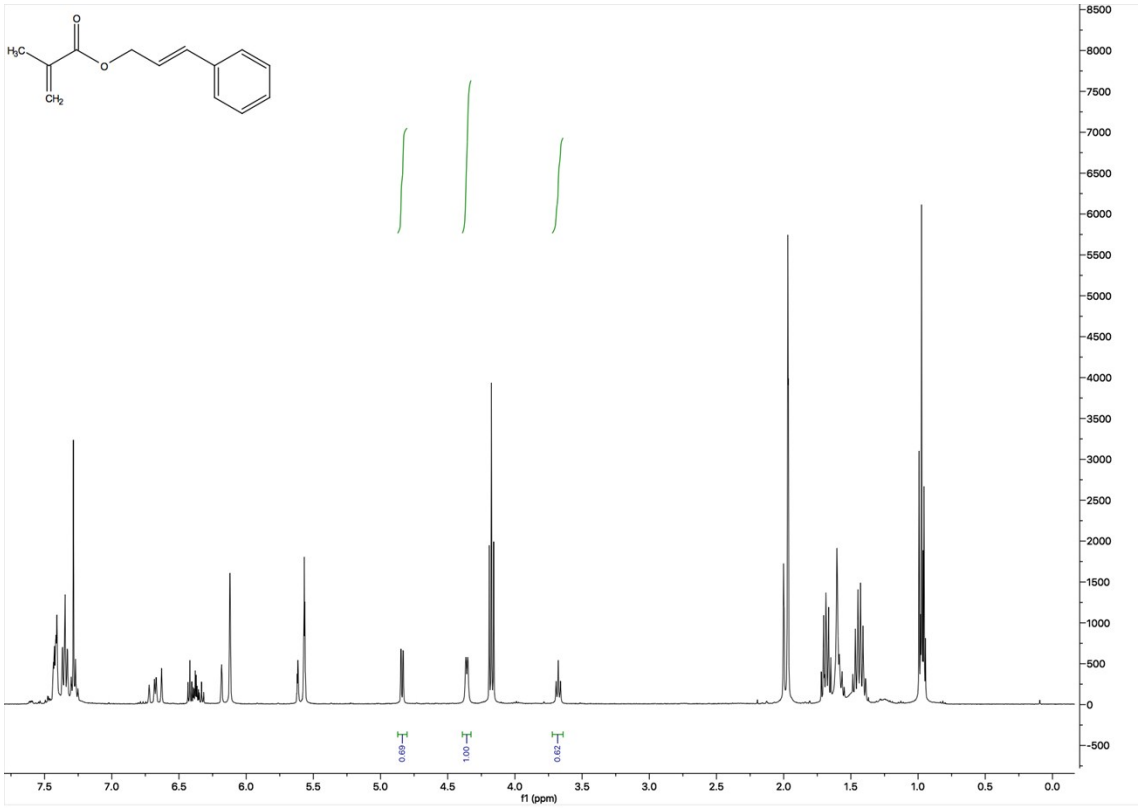

Figure S11: 1H NMR of conventional CiMA after 150 mins of heating at 160 ˚C. Conversion was shown to be 41 % by comparing proton peak change in chemical environment

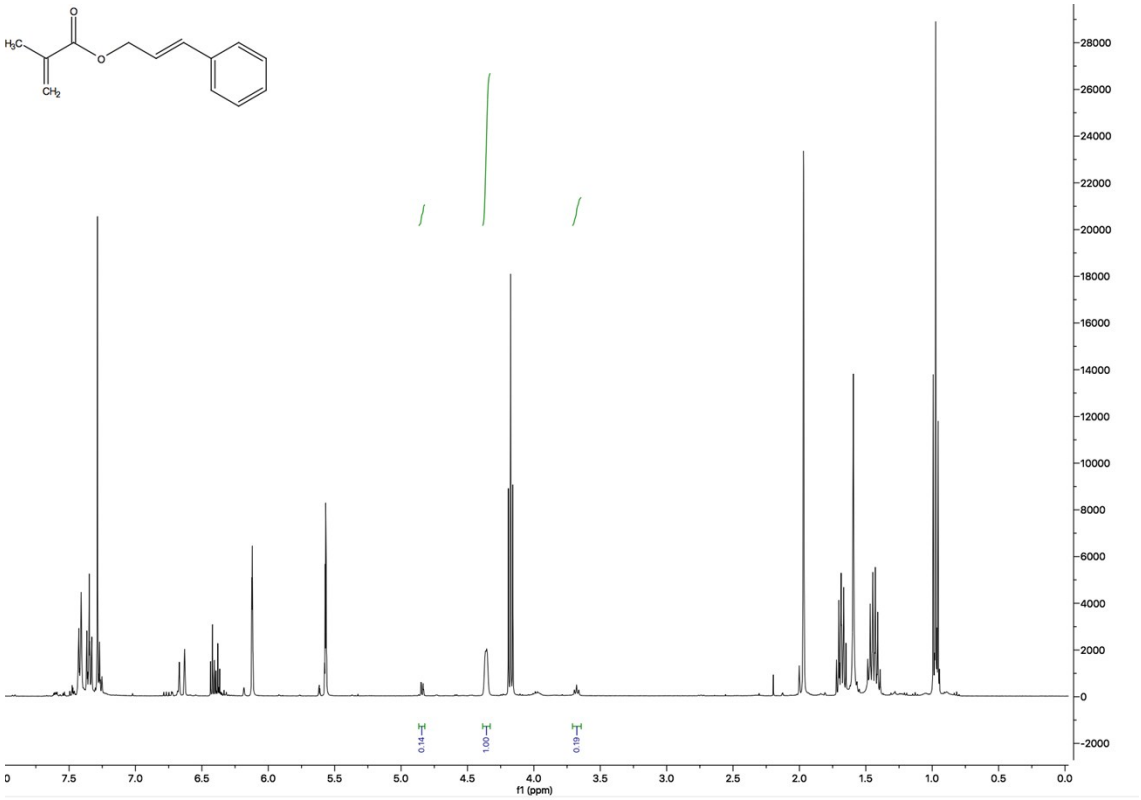

Figure S12: 1H NMR of microwave heated CiMA after 150 mins of heating at 160 ˚C. Conversion was shown to be 15 % by comparing proton peak change in chemical environment

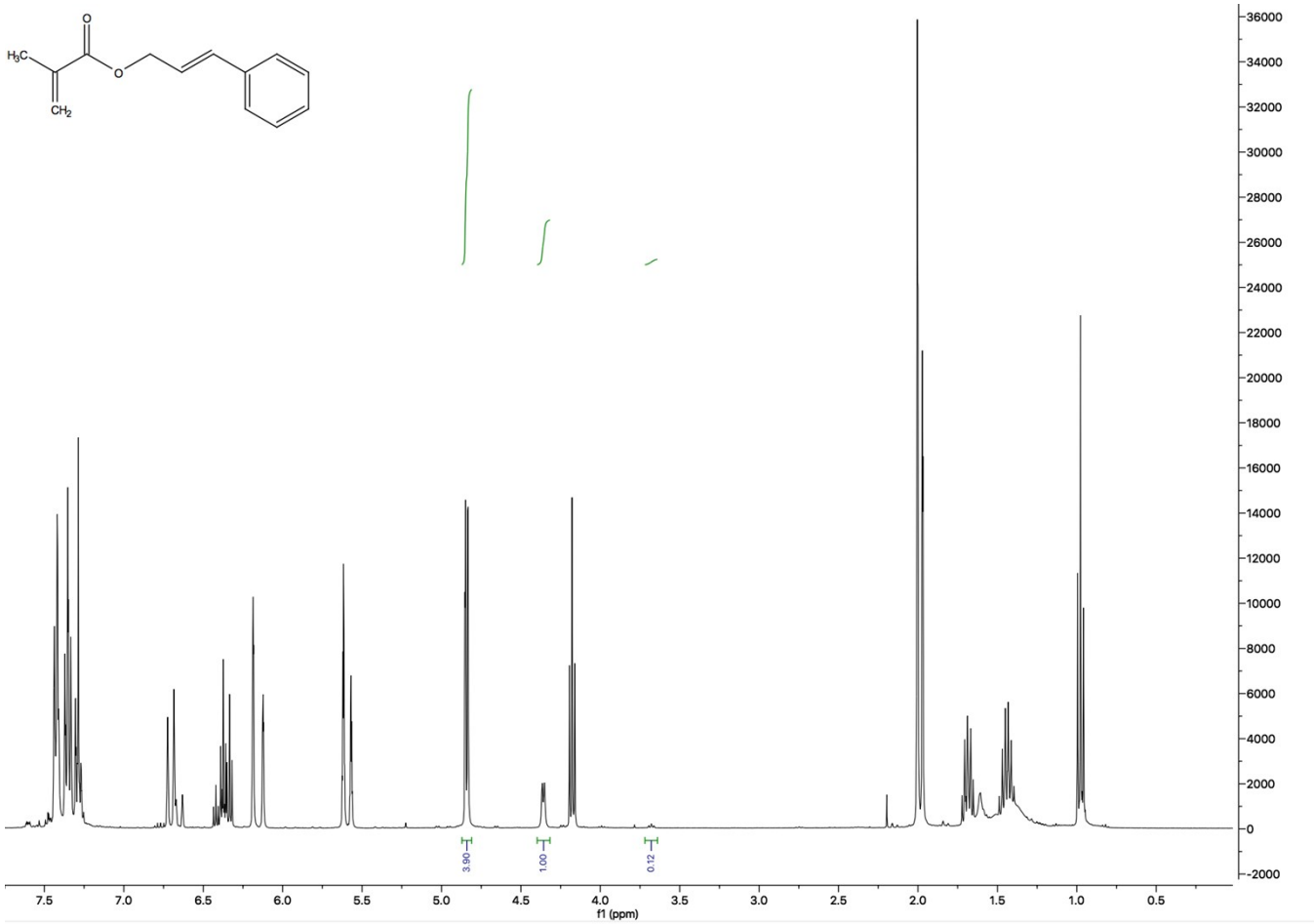

Figure S13: 1H NMR of micro-well heated CiMA after 150 mins of heating at 160 ˚C. Conversion was shown to be 80 % by comparing proton peak change in chemical environment

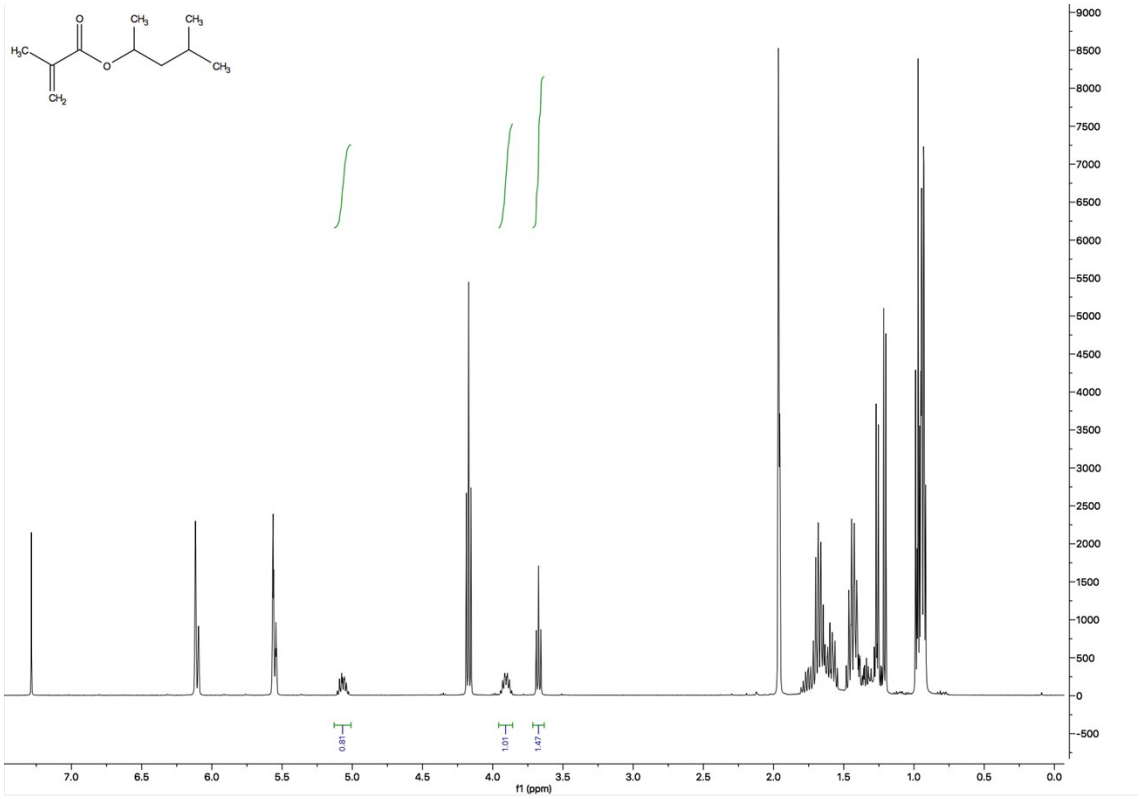

Figure S14: 1H NMR of conventionally heated MpMA after 150 mins of heating at 140 ˚C. Conversion was shown to be 45 % by comparing proton peak change in chemical environment

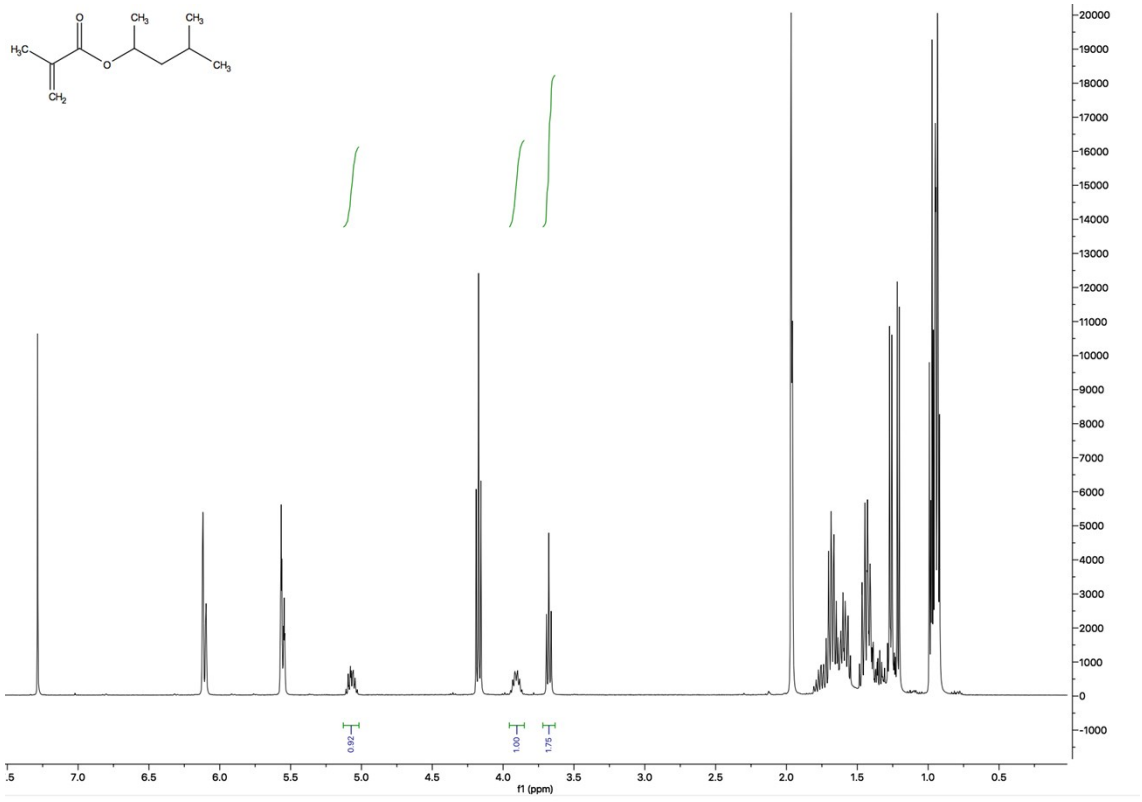

Figure S15: 1H NMR of microwave heated MpMA after 150 mins of heating at 140 ˚C. Conversion was shown to be 48 % by comparing proton peak change in chemical environment

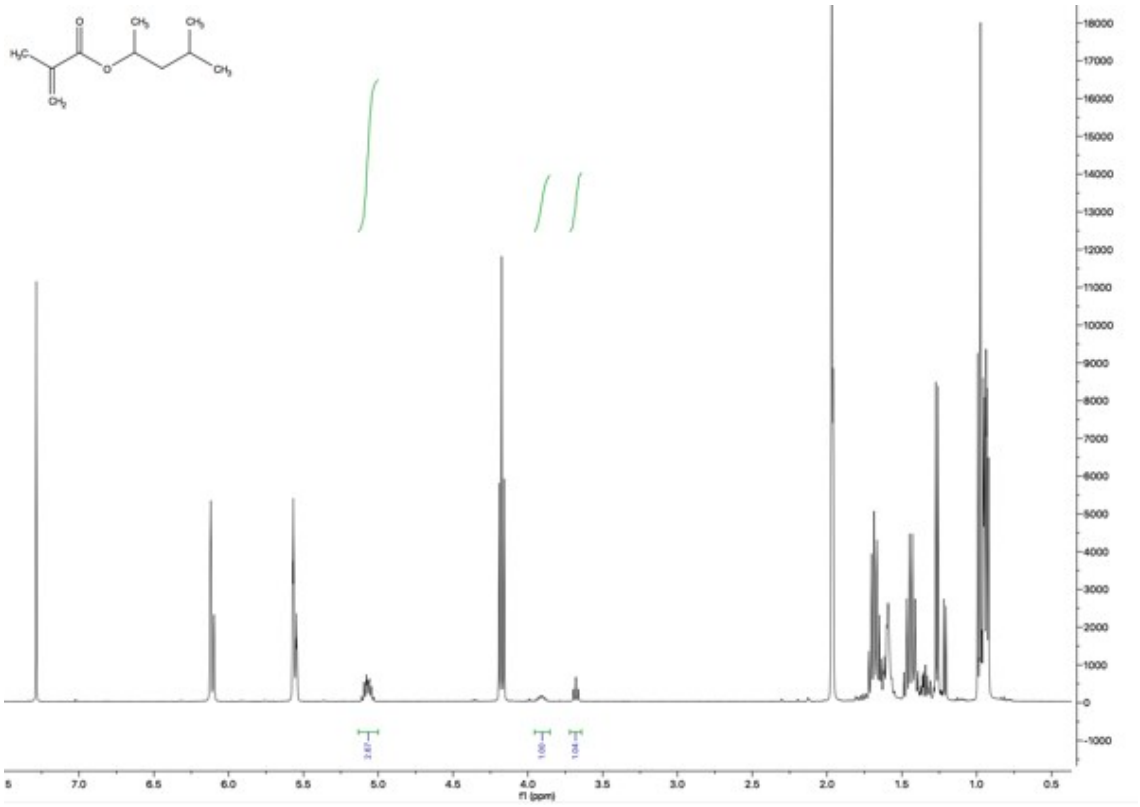

Figure S16: 1H NMR of micro-well heated MpMA after 150 mins of heating at 140 ˚C. Conversion was shown to be 73 % by comparing proton peak change in chemical environment

References

[1] T. Santos, M. A. Valente, J. Monteiro, J. Sousa, L. C. Costa, *Appl. Therm. Eng.* **2011**, *31*, 3255.